Astron. Astrophys. 319, 7–17 (1997)

ASTRONOMY
AND
ASTROPHYSICS

Deep radio observations of the "Lockman Hole"

H.R. de Ruiter[1,2], G. Zamorani[1,2], P. Parma[2], G. Hasinger[3], G. Hartner[4], J. Trümper[4], R. Burg[5], R. Giacconi[6], and M. Schmidt[7]

[1] Osservatorio Astronomico di Bologna, Via Zamboni 33, I-40126 Bologna, Italy
[2] Istituto di Radioastronomia del CNR, Via Gobetti, 101, I-40129 Bologna, Italy
[3] Astrophysikalisches Institut, An der Sternwarte 16, D-14482 Potsdam, Germany
[4] Max Planck Institut für Extra-terrestrische Physik, D-8046 Garching, Germany
[5] Space Telescope Science Institute, 3700 San Martin Drive, Baltimore, MD 21218, USA
[6] European Southern Observatory, Karl Schwarzschildstr. 2, D-8046 Garching, Germany
[7] California Institute of Technology, 105-24 Robinson Lab., Pasadena, CA 91125, USA

Received 1 March 1996 / Accepted 27 June 1996

Abstract. A deep radio image of the "Lockman Hole" is presented. The observations, done with the C-configuration of the Very Large Array at a wavelength of 20 cm, are part of a wider study of this field in X-rays with the ROSAT satellite. Optical follow up will provide a sample of objects observed down to very faint flux limits in all three wavelength windows.

The radio data reduction is described and a catalog of 149 radio sources with peak flux densities at least four times the local RMS noise is presented. The limiting peak flux density in the central part of the field is $\sim$120 μJy. The sources have been extracted from a circular area of 20′ radius around the field center.

Radio source counts are briefly discussed and shown to be in good agreement with previous results at similar flux densities.

All radio sources have been searched for optical counterparts on POSS prints and an optical candidate has been found for $\sim$30 % of the radio sources. The optical identification rate increases at fluxes $S \lesssim 0.5$ mJy and the increase is mainly due to identifications with relatively bright galaxies ($m_r < 17.5$).

Cross correlation with the X-ray source list, which contains 135 sources in the same area, yields 16 possible radio/X-ray associations. After correcting for expected spurious associations, we estimate that $\sim$ 10 % of the X-ray sources are associated with radio sources at these fluxes. Deep CCD frames provide optical counterparts for most of the radio/X-ray sources. On the basis of partial spectroscopy, optical morphology and correlations between radio, optical and X-ray fluxes, we conclude that although the majority ($\gtrsim$ 60 %) of the radio/X-ray associations are identified with AGNs, a non-negligible fraction of them ($\lesssim$ 40 %) appears to be associated with normal galaxies. Most of these galaxies have low fluxes, both in radio and in X-rays and they may partly represent the bright X-ray tail of the same population that is responsible for the upturn in the radio source counts below 1 mJy.

Key words: radio continuum: general – X-rays: general

1. Introduction

A very deep X-ray survey has recently been carried out with the ROSAT satellite in the "Lockman Hole", a region of exceptionally low HI absorption (Lockman et al. 1986). Details of the X-ray observation can be found in Hasinger et al. (1993). The 193 ksec observation reaches an unprecedented X-ray flux level of about 2×10^{-15} erg cm $^{-2}$s^{-1}, and as a result the surface density of X-ray sources is very high, of the order of 400 objects per square degree.

In the inner part of the ROSAT field a region with a radius of 20 arcmin was used to obtain a complete sample of X-ray sources; moreover this region is almost completely covered by CCD images in blue and red colors. Optical identification of the X-ray sources can therefore be attempted down to magnitudes around 24 or slightly fainter.

Deep observations in other wavelength regions, for example in the radio, are a logical follow up. Such radio observations were done with the Very Large Array and we report on them in this paper. Our aim was twofold. First, to reach faint radio flux levels and high source densities, while covering the entire central region of the ROSAT field (about a third of a square degree). Second, to use a sufficiently high angular resolution such that confusion due to the high source density would not constitute a major problem. The ideal combination is an observing wavelength of 20 cm and the C-configuration of the VLA, for which these conditions are best fullfilled.

Send offprint requests to: H.R. de Ruiter

In Sect. 2 we give a general discussion of the VLA observations. First we describe the reduction of the radio data and how we arrived at the final radio-mosaic that covers the entire X-ray field. From the radio image we extracted a sample of radio sources, which we present in the form of a table that lists some observational parameters like position, flux density and angular extent.

The search for radio counterparts of X-ray sources is described in Sect. 3, together with a preliminary search for optical counterparts of all radio sources.

Finally, in Sect. 4, we discuss the counts and sky distribution of the radio sources, and the optical and X-ray counterparts. For shortness we will denote radio sources detected only in the optical as RO, only in X-rays as RX and in the optical as well as X-rays as ROX objects.

2. The radio observations

2.1. Data reduction

The central part of the ROSAT field has a size of about 20 arcmin in radius; CCD images of a large fraction of that whole area already exist. Our aim was to cover the ROSAT area also in the radio band, without making unduly heavy demands on VLA observing time, and without complicating the reduction procedure of the radio data unnecessarily. As an optimum solution we chose for 20 cm continuum observations with the C configuration of the VLA: the A and B configurations would have drastically limited the field of view and thus many different pointings would have been necessary, while the D configuration would have provided too low a resolution. On the contrary, with the C configuration the synthesized beam is $\sim 12 - 13$ arcsec, which is adequate for our purposes. By using only four different pointing positions the flux density limit can be made reasonably uniform over the whole ROSAT field.

The observations were done in two pieces of eight hours each on November 8 and December 18, 1990 at the frequencies of 1465 and 1515 MHz with bandwidth 50 MHz. The data at the two different frequencies were kept separate in the entire reduction procedure and were combined only at the very end. Taking into account the time spent on calibrator sources the effective observing time of the ROSAT field was about twelve hours. We used four different pointing positions separated by 15 arcmin either in Right Ascension or in Declination, and situated symmetrically around the ROSAT field center, which is α(J2000) = $10^{\rm h}52^{\rm m}$, δ(J2000) = $57^{\rm o}21'36''$. Each pointing position was therefore observed for three hours. This particular choice of pointing positions was adopted in order to obtain a reasonably uniform RMS noise level over the inner 10 arcmin of the ROSAT field and a slow increase out to the ROSAT border at 20 arcmin. As will be seen below this goal was indeed achieved.

The four different pointings were calibrated separately, using 3C 286 as primary flux calibrator. The flux densities assumed for 3C 286 were 14.635 Jy at 1465 MHz and 14.399 Jy at 1515 MHz. 1031+567 was selected as secondary calibrator for the amplitudes and phases. The standard calibration procedure of the AIPS reduction package was followed. Obviously bad data were edited out first, while a check on amplitude deviations was done also after the calibration.

For each of the four fields an image of 1024×1024 pixels was constructed, using the AIPS-task MX. Since there are no very strong sources in the immediate vicinity of the Lockman Hole area it was not necessary to make the images larger than 1024×1024. A pixel-size of 2.5×2.5 arcsec was used. The images were CLEANed with the procedure built in in MX, using a restoring beam of $\sim$12 arcsec. The RMS noise levels in the eight cleaned images are uniform and of the order of 0.07 mJy (no primary beam correction applied yet), both at 1465 and 1515 MHz.

Before combining the four individual images into one mosaic, we had to take into account an effect described before by Mitchell & Condon (1985) and Kollgaard et al. (1995), who used exactly the same combination of frequency, bandwidth and VLA configuration (C) as we did. Source positions are radially squeezed towards the field center and the position shift is a function of and increases with distance from the field center. We measured a radial compression of 0.47 % by comparing the positions of sources observed in different fields. A linear correction is sufficiently accurate for the combination of the four fields, because we are using only the inner part of each radio field. Correcting for the compression reduced the discrepancies between the positions of the same sources in different fields below 1 arcsec.

One mosaic was constructed from the four images, using the AIPS task LTESS, after which the two frequencies were combined. In the inner part of the final 1024×1024 image the RMS noise is quite uniform out to a radius of 10 arcmin from the ROSAT field center, at a level of ~ 30 μJy, and after that it starts to degrade reaching $\sim$55 μJy at the outer edge of the X-ray field, at 20 arcmin from the center of the radio mosaic. Measurements of the RMS noise at various distances from the field center are shown in Fig. 1, together with a second order polynomial fit. A check was made for a possible azimuthal component of the noise but none was found.

2.2. The radio catalog

In order to construct the radio catalog, we first extracted all pixels with a peak flux density at least four times the *local* RMS noise from the inner region with a radius of 20 arcmin around the center of the mosaic. At these positions we then made gaussian fits to determine the source extent and the total flux density. In very few cases the source was so extended that a simple gaussian fit was not possible: the flux density was then determined by summing the values of all the pixels covering the source. Given the number of independent resolution elements in the image, our choice of a 4σ threshold in $S_{\rm peak}$ implies that $\sim$ 1 spurious source may be present in this sample of radio sources. Allowing for some possible spatial correlation in the map noise, the number of spurious sources due to noise only is expected to be at most a few. It is well known that at this

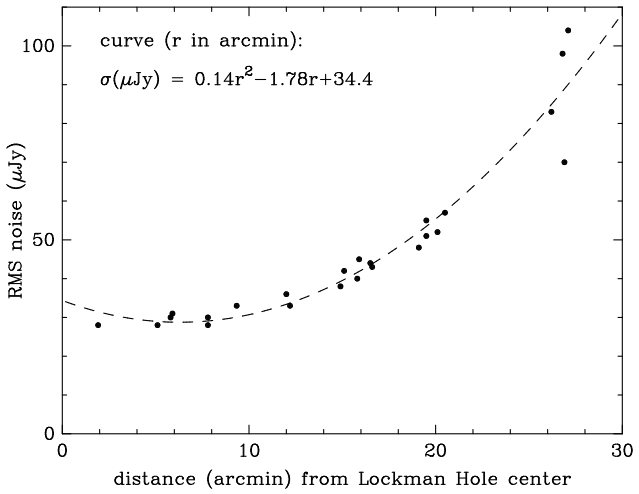

Fig. 1. The RMS noise (in μJy) as a function of distance from the image center. No azimuthal component was found. The broken line is a quadratic best fit, which, however, slightly exaggerates the increase of the noise towards the field center. The actual measurements show a plateau with $\sigma \sim 30$ μJy all the way to the center.

level an accurate determination of completeness and reliability of a sample of radio sources is problematic, due to the presence of faint ($< 4\sigma$) sources, whose flux densities may be boosted by noise-fluctuations above the 4σ limit. Therefore, when e.g. constructing source counts one should use a higher limit (at least, say, 5σ, see in particular Sect. 4).

The resulting list of radio sources has 149 entries, and is given in Table 1. Column 1 gives a running number. In columns 2 and 3 right ascension and declination for epoch J2000 are given, followed by the *total* flux density at 1.5 GHz in column 4. An asterisk after the flux density indicates that the *peak* flux density is between 4 and 5 times the local RMS noise. The largest angular size and its position angle are given in columns 5 and 6. The errors in position and flux density were determined following the recipe given by Kollgaard et al (1995). Note that the internal position errors do not account for absolute errors which may be of the order of 1 to 2 arcsec. We therefore added an error of 1.5 arcsec in quadrature, and this is the total position error given in Table 1.

We do not give an error estimate of the angular size and position angle: while the formal uncertainties of the gaussian fits are usually of the order of one arcsec, other errors, e.g. due to bandwidth smearing, may be more important but hard to estimate.

Some sources in Table 1 are listed as double or triple. The decision to consider two or three components as belonging to a single source is somewhat ambiguous. In a few cases (see e.g. sources 57 and 71) the probability that we deal with genuine double or triple sources is quite high, but in other cases the classification as double source is purely based on the small separation between the components and the approximate equality of their flux densities (e.g. source 99). Considering the high

Table 1. The 4σ radio sample

Nr	RA (2000)	DEC (2000)	Flux Density *mJy*	LAS *arcsec*	PA *degr*
1	10 49 43.70± 0.22	57 17 36.3± 1.7	0.88± 0.10	<17.9	
2	10 49 51.18± 0.21	57 28 11.4± 1.6	1.01± 0.10	17.3	97
3	10 49 53.07± 0.29	57 26 15.6± 2.1	0.11± 0.05*	u	
4	10 50 08.02± 0.19	57 20 16.2± 1.5	1.74± 0.10	13.5	120
5	10 50 12.73± 0.21	57 11 37.7± 1.7	0.60± 0.06	u	
6	10 50 14.43± 0.25	57 28 44.2± 1.9	0.34± 0.05	u	
7	10 50 15.58± 0.28	57 13 14.9± 2.0	0.22± 0.05*	u	
8	10 50 19.15± 0.24	57 28 37.7± 1.9	0.22± 0.04	u	
9	10 50 19.36± 0.25	57 28 11.6± 1.9	0.32± 0.04	u	
10	10 50 23.08± 0.27	57 24 40.7± 2.0	0.22± 0.04*	u	
11	10 50 25.24± 0.25	57 33 13.8± 1.9	0.31± 0.05	u	
12	10 50 26.31± 0.22	57 07 44.2± 1.7	0.76± 0.09	13.9	30
13	10 50 27.30± 0.27	57 21 15.5± 2.0	0.17± 0.04*	u	
14	10 50 29.14± 0.19	57 14 27.1± 1.5	1.18± 0.06	u	
15	10 50 31.80± 0.21	57 20 26.3± 1.6	0.90± 0.08	15.1	157
16	10 50 32.53± 0.21	57 26 45.4± 1.7	0.35± 0.04	u	
17	10 50 32.94± 0.29	57 35 31.1± 2.1	0.31± 0.05*	u	
18	10 50 33.96± 0.25	57 29 22.1± 1.9	0.34± 0.04	u	
19	10 50 33.97± 0.19	57 21 52.2± 1.6	0.91± 0.06	9.6	108
20	10 50 34.26± 0.26	57 15 22.6± 2.0	0.22± 0.04	u	
21	10 50 35.66± 0.27	57 26 01.6± 2.0	0.14± 0.03*	u	
22	10 50 35.97± 0.19	57 23 19.4± 1.5	1.63± 0.08	12.1	32
23	10 50 37.19± 0.21	57 37 40.2± 1.7	0.62± 0.06	u	
24	10 50 37.56± 0.23	57 28 43.2± 1.8	0.37± 0.05	10.1	90
25	10 50 39.47± 0.19	57 23 35.9± 1.5	4.05± 0.14	8.5	9
26	10 50 40.66± 0.20	57 33 07.6± 1.6	0.57± 0.05	u	
27	10 50 41.82± 0.23	57 07 05.8± 1.8	0.58± 0.07	<12.1	
28	10 50 45.08± 0.21	57 37 34.7± 1.6	1.05± 0.10	15.2	133
29	10 50 50.49± 0.24	57 07 14.1± 1.8	0.46± 0.05	u	
30	10 50 52.45± 0.27	57 35 06.5± 2.0	0.29± 0.06*	<13.5	
31	10 50 53.37± 0.23	57 24 26.6± 1.8	0.22± 0.03	u	
32	10 50 54.82± 0.26	57 08 09.9± 2.0	0.33± 0.05	u	
33	10 50 56.26± 0.24	57 16 31.1± 1.9	0.27± 0.04	<9.5	
34	10 50 56.46± 0.19	57 15 32.0± 1.6	0.78± 0.05	8.0	91
35	10 50 57.40± 0.25	57 29 56.3± 1.9	0.15± 0.03	u	
36	10 51 00.93± 0.24	57 20 35.5± 1.8	0.25± 0.03	<7.2	
37	10 51 01.79± 0.20	57 34 46.3± 1.6	0.94± 0.06	<12.0	
38	10 51 05.80± 0.19	57 10 56.4± 1.7	0.43± 0.05	<8.2	
39	10 51 06.85± 0.22	57 11 52.4± 1.7	0.37± 0.04	u	
40	10 51 10.29± 0.30	57 16 03.1± 2.2	0.12± 0.03*	u	
41	10 51 13.59± 0.25	57 26 53.9± 1.9	0.22± 0.03	u	
42	10 51 13.39± 0.19	57 14 25.7± 1.6	0.62± 0.04	u	
43	10 51 14.95± 0.19	57 35 52.0± 1.5	1.94± 0.09	8.4	158
44	10 51 17.63± 0.20	57 16 38.0± 1.6	0.50± 0.03	u	
45	10 51 20.30± 0.22	57 22 52.6± 1.7	0.24± 0.03	u	
46	10 51 20.82± 0.19	57 35 32.3± 1.5	7.56± 0.29	8.9	168
47*	10 51 20.34± 0.22	57 09 51.7± 1.7	0.58± 0.10	39.1	153
47a	10 51 19.70	57 10 09.4	0.17		
47b	10 51 20.34	57 09 51.7	0.41		
48	10 51 20.79± 0.21	57 30 36.8± 1.6	0.36± 0.03	u	
49	10 51 22.04± 0.19	57 08 54.0± 1.5	9.91± 0.37	9.0	29
50	10 51 22.91± 0.19	57 32 28.1± 1.5	1.25± 0.06	6.3	170
51	10 51 25.62± 0.22	57 35 42.8± 1.7	0.45± 0.05	7.0	156
52	10 51 25.96± 0.27	57 21 53.9± 2.0	0.19± 0.04*	<10.2	
53	10 51 27.99± 0.30	57 39 25.2± 2.2	0.16± 0.05*	u	
54	10 51 27.94± 0.22	57 35 00.8± 1.7	0.37± 0.04	u	
55	10 51 27.81± 0.19	57 08 59.5± 1.5	11.73± 0.44	16.1	20
56	10 51 30.41± 0.28	57 38 08.0± 2.0	0.23± 0.04*	u	
57*	10 51 29.97± 0.19	57 11 44.2± 1.5	10.85± 0.46	129.7	146
57a	10 51 27.43	57 12 16.7	2.78		
57b	10 51 32.53	57 11 12.2	8.07		
58	10 51 34.03± 0.24	57 09 22.4± 1.9	0.41± 0.06	14.0	53
59	10 51 35.65± 0.27	57 27 37.8± 2.0	0.19± 0.03	u	
60	10 51 36.20± 0.20	57 33 02.2± 1.6	0.45± 0.04	u	
61	10 51 36.39± 0.22	57 29 55.6± 1.7	0.40± 0.05	<15.1	
62	10 51 36.96± 0.21	57 37 52.0± 1.7	0.42± 0.05	u	
63	10 51 37.00± 0.19	57 29 40.2± 1.5	2.21± 0.08	6.2	62
64	10 51 39.17± 0.22	57 30 44.8± 1.7	0.45± 0.05	<15.2	
65	10 51 41.40± 0.22	57 19 51.6± 1.7	0.29± 0.03	u	
66	10 51 41.92± 0.19	57 36 01.2± 1.5	4.76± 0.19	15.1	176
67	10 51 41.99± 0.20	57 34 48.3± 1.6	0.55± 0.04	u	
68	10 51 42.18± 0.26	57 15 00.2± 1.9	0.15± 0.03	u	
69	10 51 43.64± 0.21	57 29 35.6± 1.6	0.42± 0.04	10.8	117
70	10 51 44.42± 0.27	57 17 18.0± 2.0	0.19± 0.03*	u	

Table 1. (continued)

Nr	RA (2000)	DEC (2000)	Flux Density *mJy*	LAS *arcsec*	PA *degr*
71*	10 51 48.72± 0.19	57 32 48.2± 1.5	15.39± 0.58	137.5	127
71a	10 51 44.28	57 33 13.6	11.65		
71b	10 51 48.72	57 32 48.2	0.75		
71c	10 51 55.54	57 32 07.0	2.98		
72	10 51 49.88± 0.26	57 26 36.1± 2.0	0.22± 0.06	25.0	90
73	10 51 52.36± 0.19	57 09 49.6± 1.5	2.96± 0.11	8.0	80
74	10 51 58.93± 0.24	57 23 30.9± 1.9	0.19± 0.03	u	
75	10 52 00.29± 0.30	57 24 20.3± 2.2	0.13± 0.03*	u	
76	10 52 01.62± 0.30	57 40 49.4± 2.2	0.21± 0.05*	u	
77	10 52 06.41± 0.19	57 41 09.3± 1.5	10.25± 0.50	15.3	5
78	10 52 07.05± 0.25	57 07 44.0± 1.9	0.20± 0.04	u	
79	10 52 07.49± 0.22	57 19 02.7± 1.7	0.29± 0.04	<9.4	
80	10 52 10.52± 0.26	57 12 02.8± 2.0	0.16± 0.03	u	
81	10 52 11.01± 0.19	57 29 07.6± 1.5	1.46± 0.06	9.4	91
82	10 52 12.08± 0.30	57 15 48.0± 2.2	0.10± 0.03*	u	
83	10 52 12.40± 0.23	57 24 49.7± 1.8	0.27± 0.03	u	
84	10 52 13.30± 0.22	57 16 04.5± 1.7	0.31± 0.03	u	
85	10 52 17.12± 0.27	57 35 29.3± 2.0	0.21± 0.04*	u	
86	10 52 17.68± 0.26	57 21 25.0± 1.9	0.18± 0.03	u	
87	10 52 24.27± 0.19	57 08 38.4± 1.5	2.52± 0.11	14.4	113
88	10 52 25.10± 0.26	57 11 30.5± 2.0	0.12± 0.03	u	
89	10 52 25.59± 0.19	57 33 22.1± 1.5	4.51± 0.16	9.9	90
90	10 52 25.64± 0.29	57 22 47.0± 2.2	0.10± 0.03*	u	
91	10 52 26.64± 0.29	57 27 59.3± 2.1	0.16± 0.03*	u	
92	10 52 29.41± 0.27	57 12 40.0± 2.0	0.19± 0.03*	u	
93	10 52 30.49± 0.22	57 13 10.6± 1.7	0.31± 0.03	u	
94	10 52 30.47± 0.23	57 08 52.2± 1.8	0.26± 0.04	u	
95	10 52 31.01± 0.27	57 34 58.1± 2.0	0.20± 0.04*	u	
96	10 52 31.78± 0.19	57 06 49.7± 1.6	1.23± 0.08	10.4	38
97	10 52 32.35± 0.28	57 08 42.3± 2.1	0.26± 0.05*	11.4	68
98	10 52 35.34± 0.23	57 26 49.0± 1.8	0.35± 0.05	<18.0	
99*	10 52 37.17± 0.19	57 31 02.7± 1.5	59.45± 1.91	63.7	26
99a	10 52 36.44	57 30 48.8	34.15		
99b	10 52 38.02	57 31 16.2	25.30		
100	10 52 39.42± 0.27	57 24 29.8± 2.0	0.14± 0.03*	u	
101	10 52 41.43± 0.19	57 23 19.8± 1.5	1.72± 0.07	9.4	88
102	10 52 42.27± 0.22	57 24 43.2± 1.8	0.22± 0.03	u	
103	10 52 42.55± 0.22	57 19 14.8± 1.7	0.25± 0.03	u	
104	10 52 45.01± 0.23	57 36 16.4± 1.8	0.46± 0.06	14.3	84
105	10 52 52.39± 0.23	57 28 58.8± 1.8	0.20± 0.03	u	
106	10 52 52.62± 0.24	57 07 53.1± 1.9	0.28± 0.04	u	
107	10 52 53.30± 0.28	57 27 00.8± 2.0	0.13± 0.03*	u	
108	10 52 53.80± 0.27	57 18 23.6± 2.0	0.17± 0.03*	u	
109	10 52 55.27± 0.19	57 19 49.8± 1.5	2.69± 0.09	8.7	28
110	10 52 56.34± 0.24	57 23 59.7± 1.9	0.19± 0.03	u	
111*	10 52 57.20± 0.21	57 08 29.9± 1.7	0.60± 0.07	19.5	40
111a	10 52 56.73	57 08 25.0	0.30		
111b	10 52 57.67	57 08 34.9	0.30		
112	10 52 57.77± 0.27	57 15 15.6± 2.0	0.18± 0.03*	u	
113	10 52 59.47± 0.23	57 32 23.9± 1.8	0.28± 0.04	<8.7	
114	10 53 01.72± 0.26	57 25 20.8± 1.9	0.15± 0.03	u	
115	10 53 01.34± 0.20	57 05 42.7± 1.6	0.93± 0.06	u	
116	10 53 03.78± 0.22	57 35 32.0± 1.8	0.37± 0.04	u	
117	10 53 03.71± 0.22	57 12 05.5± 1.7	0.36± 0.04	u	
118	10 53 04.16± 0.25	57 15 46.0± 1.9	0.19± 0.03	u	
119	10 53 04.80± 0.20	57 30 55.6± 1.6	0.44± 0.04	u	
120	10 53 07.75± 0.28	57 15 03.2± 2.0	0.18± 0.03*	u	
121	10 53 08.12± 0.22	57 22 22.9± 1.7	0.34± 0.03	u	
122	10 53 08.26± 0.22	57 16 57.8± 1.7	0.43± 0.05	15.4	106
123	10 53 09.25± 0.30	57 37 11.3± 2.2	0.17± 0.05*	u	
124	10 53 09.34± 0.22	57 06 36.7± 1.7	0.56± 0.05	u	
125	10 53 12.09± 0.22	57 11 05.4± 1.7	0.59± 0.07	16.9	127
126	10 53 12.53± 0.23	57 31 12.1± 1.8	0.23± 0.04	u	
127	10 53 14.01± 0.22	57 30 18.7± 1.7	0.29± 0.04	u	
128	10 53 16.62± 0.29	57 35 50.4± 2.1	0.25± 0.05*	u	
129	10 53 18.84± 0.21	57 21 41.1± 1.6	0.35± 0.03	u	
130	10 53 19.08± 0.20	57 18 51.4± 1.6	0.61± 0.04	7.6	39
131	10 53 19.53± 0.27	57 12 45.0± 2.0	0.17± 0.04*	u	
132	10 53 22.95± 0.21	57 15 01.2± 1.7	0.50± 0.05	12.6	74
133	10 53 24.60± 0.20	57 16 57.7± 1.6	0.56± 0.04	6.8	97
134	10 53 25.18± 0.20	57 29 10.7± 1.6	0.55± 0.04	6.4	20
135	10 53 26.47± 0.23	57 14 04.3± 1.8	0.30± 0.04	<5.9	
136	10 53 27.45± 0.28	57 09 31.7± 2.1	0.35± 0.07*	u	
137	10 53 27.91± 0.24	57 11 14.6± 1.8	0.23± 0.04	u	

Table 1. (continued)

Nr	RA (2000)	DEC (2000)	Flux Density *mJy*	LAS *arcsec*	PA *degr*
138	10 53 35.10± 0.24	57 29 20.0± 1.8	0.21± 0.04	u	
139	10 53 40.67± 0.28	57 26 27.0± 2.0	0.13± 0.04*	u	
140	10 53 40.75± 0.27	57 19 19.3± 2.0	0.18± 0.04*	u	
141	10 53 40.87± 0.19	57 19 52.7± 1.5	1.46± 0.07	7.9	30
142	10 53 42.02± 0.23	57 30 25.4± 1.8	0.27± 0.04	u	
143	10 53 43.60± 0.27	57 25 31.1± 2.0	0.22± 0.04*	u	
144	10 53 47.94± 0.25	57 17 36.6± 1.9	0.39± 0.06	<17.2	
145	10 53 56.31± 0.27	57 22 41.7± 2.0	0.18± 0.04*	u	
146	10 54 00.50± 0.19	57 33 20.8± 1.5	2.86± 0.15	u	
147	10 54 05.97± 0.28	57 24 13.6± 2.0	0.21± 0.04*	u	
148	10 54 06.65± 0.19	57 12 56.6± 1.5	1.76± 0.11	13.4	120
149	10 54 21.05± 0.20	57 25 43.7± 1.6	0.80± 0.07	7.2	98

density of sources in the Lockman Hole field it is possible that for one or two sources the components are in reality unrelated radio sources.

A "u" in column 5 stands for "unresolved". For faint sources ($S_{1.5} < 0.2$ mJy) this means that the source may in reality be as large as the synthesized beam ($\sim$ 12 arcsec), while for the strongest sources ($S_{1.5} > 1$ mJy) the implied size is smaller than a few arcsec.

The question of the sample completeness is a highly complicated one, especially if the detection criterion is based on a peak flux density of less than about ten times the RMS noise. An extensive discussion of completeness, taking into account detection limit and angular size distribution can be found in Windhorst et al. (1984); see also Fomalont et al. (1991). Accurate statistical corrections can be applied to e.g. source counts. Unfortunately, when trying to identify X-ray sources with individual radio sources such a statistical approach is not valid, and the problem of completeness has to be kept in mind in the following when we give identification percentages of RX and ROX objects – those numbers should be considered as indicative, and perhaps only as lower limits. Although never explicitly stated, this same problem plagues similar studies, where radio counterparts of X-ray sources are sought down to the $\sim 4-5\sigma$ level (e.g. Warwick & Barber 1992, Boyle et al. 1993).

For easy reference we visualize in Fig. 2 the radio sources in the 4σ sample. The circle is drawn at a radius of 20 arcmin from the field center; its interior covers the entire region of the complete ROSAT X-ray sample. Different symbols are used for faint ($S_{1.5} < 0.325$ mJy) and bright ($S_{1.5} > 0.325$ mJy) sources, where 0.325 mJy is the median flux density of the sample. The latter sources would be detectable above the 4σ level in the whole area of 20 arcmin radius and their sky distribution can therefore be analyzed for possible clustering (see Sect. 4.1).

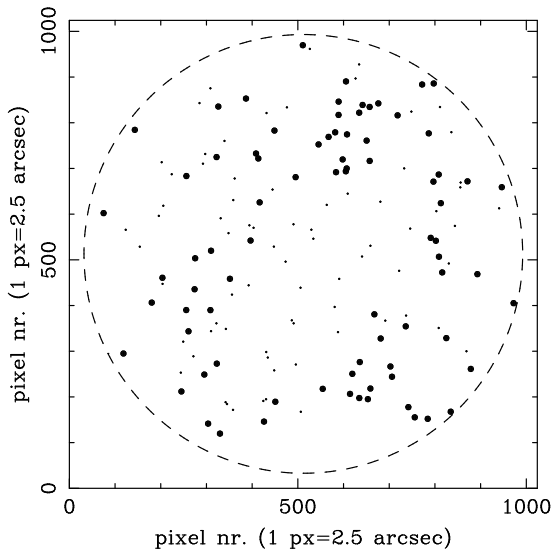

Fig. 2. The sources of the 4σ radio sample. The circle has a radius of 20 arcminutes and indicates (approximately) the area covered by the complete ROSAT X-ray sample. Sources with flux density above 0.325 mJy (the median flux density of the sample) are represented by filled circles. Such sources would be visible in the whole 40 arcmin diameter area and can therefore be used to study their sky distribution. The fainter sources are indicated by the dots; those with $S_{1.5} < 0.21$ mJy have visibility areas that depend on their flux density and therefore their apparent sky distribution is not representative of the true distribution.

3. Radio, optical and X-ray associations

3.1. Radio identification of X-ray sources

The X-ray list of the Lockman Hole field, which is still subject to possible minor modifications, contains $\sim$ 135 sources down to $\sim 2\times10^{-15}$ erg cm^{-2}s^{-1} in the 0.5–2 keV band within a radius of 20 arcmin from the ROSAT pointing center (Hasinger et al., in preparation). A cross correlation was performed between the positions of the X-ray sources and the 149 radio sources of the 4σ sample. We used the likelihood ratio (LR) as our criterion for accepting or rejecting a possible identification; LR compares the probabilities that, given a certain positional difference and the position errors in the two bands, a radio object is respectively a true identification or an unrelated background object. An object is accepted as identification if its LR is larger than a certain cutoff value $(LR)_{\rm min}$. The cutoff value is chosen a posteriori and depends on the quality one requires of the identification sample. For each cutoff value it is possible to quantitatively estimate the completeness (C) of the proposed identification sample and its reliability (R), i.e. the amount of contamination with spurious background objects. From the observed fraction of identifications, $\theta_{\rm obs} = N(LR > (LR)_{\rm min})/N$(X-ray sources), the *true* identification rate can be determined: $\theta_{\rm true} = (R/C)\theta_{\rm obs}$. For more details we refer to de Ruiter et al. (1977) and Willis & de Ruiter (1977).

In order to be able to evaluate the quality of the identifications one needs to have some realistic estimate of the uncertainties in both the radio and X-ray positions. The radio position errors were discussed in Sect. 2.2; a similar procedure (i.e. adding in quadrature statistical and absolute errors) has been adopted for the errors in the X-ray positions. The final error used in the calculation of the likelihood ratio is the combination of the radio and X-ray errors: $\sigma_{\rm T} = \sqrt{\sigma^2_{\rm RT} + \sigma^2_{\rm XT}}$.

Cross-correlation of the list of X-ray sources and the 4σ radio sample results in 15 radio/X associations with $LR > 5$, while an additional probable association (X28/R149) has been added in the final list of Table 2 (see below). Following the recipe given by de Ruiter et al. (1977) the completeness and reliability of the identifications are determined in a straightforward way. We find $C = 0.97$, so that no more than one true radio/X association, and most likely none, should have been missed because of a large difference between the radio and X positions. The reliability is $R = 0.83$: we expect that about two proposed identifications are in reality spurious positional coincidences of unrelated radio and X-ray objects. A lower cutoff, $(LR)_{\rm min} < 5$, would have resulted in a much worse reliability ($R < 0.8$), and, consequently, in an unacceptably low quality of the identification sample.

Using the 14 radio/X-ray associations with $LR > 10$, of which at most one is expected to be spurious, we find that the average radio minus X-ray positions are $\Delta\alpha = 0.0 \pm 1.4$ arcsec and $\Delta\delta = -1.5 \pm 1.2$ arcsec, showing that the coordinate systems in the two bands are well consistent with each other.

The radio/X-ray associations are given in Table 2: in column 1 and 2 the X and radio number are listed, followed by the X-ray positions at epoch J2000 in columns 3 and 4; in columns 5 and 6 the X-ray flux (in 10^{-14} erg cm^{-2}s^{-1}) between 0.5 and 2 keV and the radio flux density at 1.5 GHz in mJy. The distance to the ROSAT field center is listed in column 7 and the positional differences (in the sense radio minus X) in columns 8 and 9. The likelihood ratio, in column 10, should give some idea about the firmness of each radio/X association. It will be noted that one object has been added as the sixteenth identification even though its likelihood ratio is practically zero. The reason is that an X-ray position based on the hard X-ray band coincides within a second of arc with the radio position and in particular with the optical position of an 18th magnitude AGN. The X-ray position quoted in Table 2, which was derived after a deblending procedure, may be slightly off due to its closeness to the ribs of the ROSAT PSPC structure.

3.2. Optical identification of RX sources

Almost the entire ROSAT field is covered by CCD images in two colors, b and r, although for a few X-ray sources a finding chart is not available at present (in fact, it is absent for two RX sources in Table 3). For those that do have a finding chart all optical objects located within a radius of $\sim$ 30 arcsec from the X-ray position were selected, classified according to type (galaxy, stellar, fuzz, etc.), and their positions and blue and red magnitudes determined. The magnitude limits are, very roughly, of the order of 24 on both the blue and red images. Without radio information the identification process of faint X-ray sources with faint

Table 2. Radio/X-ray associations

X	R	RA (2000)	DEC (2000)	F_X	S_R	Off-Axis *arcm*	$\Delta\alpha$ *arcs*	$\Delta\delta$ *arcs*	L.R.
26	9	10 50 20.3	57 28 07.1	1.08	0.32	15.4	–7.5	4.5	30.4
35	25	10 50 39.2	57 23 39.3	1.33	4.05	11.9	2.2	–3.4	203.8
50	33	10 50 54.9	57 16 32.1	0.42	0.27	11.5	11.1	–1.0	11.1
87	39	10 51 06.5	57 12 00.2	0.48	0.37	13.4	2.8	–7.8	52.7
63	49	10 51 23.3	57 09 01.1	0.77	9.91	14.9	–10.2	–7.1	6.1
418	66	10 51 41.9	57 35 54.4	0.23	4.76	13.7	0.2	6.8	60.7
12	71	10 51 49.2	57 32 51.3	1.41	15.39	10.4	–3.9	–3.1	140.1
33	75	10 52 00.3	57 24 19.0	0.36	0.13	2.1	0.1	1.4	193.0
1	77	10 52 06.4	57 41 18.6	1.03	10.25	18.7	0.1	–9.3	37.1
116	99	10 52 38.1	57 31 06.5	0.51	59.45	10.4	–7.5	–3.8	25.2
32	100	10 52 39.9	57 24 32.4	5.85	0.14	4.8	–3.9	–2.6	166.9
438	109	10 52 54.9	57 19 52.9	0.23	2.69	7.0	3.0	–3.1	143.5
54	120	10 53 07.0	57 15 05.0	1.01	0.18	11.1	6.1	–1.8	74.1
6	128	10 53 17.1	57 35 49.1	7.94	0.25	16.1	–3.9	1.3	258.9
45	130	10 53 18.9	57 18 51.2	0.94	0.61	10.4	1.4	0.2	382.8
28	149	10 54 20.3	57 25 59.1	9.26	0.80	18.1	6.1	–15.4	0.0

Table 3. Optical counterparts of RX sources

X Number	R	Type	b	r	$b-r$	$\Delta\alpha$ *arcs*	$\Delta\delta$ *arcs*	Shift	$L.R.$	I.D.	Comments
26	9	g	19.58	18.69	0.89	–0.9	–0.8	*	21.7	yes	NELG (AGN)
35	25	s	19.29	18.92	0.37	0.7	0.3	*	23.9	yes	AGN
50	33	g	21.99	20.17	1.82	–2.7	0.7		10.1	yes	1
87	39	g	21.31	19.96	1.35	3.0	0.6		8.1	yes	2
63	49	g	24.55	–	–	9.4	–2.1		0.0	no	
418	66	No CCD finding chart; empty field on POSS									
12	71	s	–	22.89	–	1.1	0.8	*	20.4	yes	AGN
33	75	g	22.97	22.24	0.74	0.9	0.6	*	22.3	yes	3; galaxy
1	77	No CCD finding chart; empty field on POSS									
116	99	g	–	20.87	–	–0.9	–0.7	*	22.3	yes	4; g. in cluster
32	100	s	18.83	18.10	0.73	–0.5	–0.5	*	24.4	yes	AGN
438	109	g?	24.51	23.06	1.45	–0.1	5.7		0.5	no	
54	120	s	22.43	21.80	0.63	–0.3	3.9		4.2	yes	5; AGN
6	128	s	19.15	18.41	0.74	–0.5	0.8	*	23.4	yes	AGN
45	130	g?	–	21.00:	–	0.7	0.5	*	23.4	yes	6
28	149	s	–	18.22	–	–0.9	0.6		–	yes	7; AGN

Comments to Table 3:

1. **X 50**: a second faint galaxy (r = 23.52) is also very close, at 4.7 arcsec from the radio source.
2. **X 87**: a second galaxy with b = 21.77 and r = 20.61 is also very close, at 3.2 arcsec from the radio source.
3. **X 33**: a stellar object with b = 22.53 and r = 21.79 is also close: $\Delta\alpha = -4.1$, $\Delta\delta = -4.8$.
4. **X 116**: the radio source is very extended ($\approx$ 1 arcmin).

Another very blue object (b = 21.76) may be a good candidate. It has a radio–optical positional difference of (–6.5, –10.6), and is close to the position of one of the radio components (see Table 1).

5. **X 54**: a second stellar object is also very close, at 4.7 arcsec from the radio position.
6. **X 45**: The magnitude is an eye estimate. There is a spectroscopically confirmed AGN, with r = 20.24, at $\Delta\alpha = -8.2$ arcsec and $\Delta\delta = -0.5$ arcsec.
7. **X 28**: There is a hard-X ray position (α = 10 : 54 : 21.1, δ = 57 : 25 : 41.7), which coincides very well with the radio and optical position.

optical candidates is rather complicated, because usually more than one optical candidate can be found inside the X-ray error box. The presence of a radio position restricts the search area considerably and in most cases only one good optical candidate remains. A complication, found during the optical identification process, is a systematic shift of about four arcsec in right ascension between the optical and the radio and X-ray coordinates. We tried to correct for the shift as follows. Using only the radio and optical positions, we selected a subsample of the RX sources for which a constant shift between optical and radio positions produces unambiguous optical identifications within 1.5 arcsec. These objects, identified by an asterisk in Table 3, were used to compute the shifts in α and δ, which were then subtracted from all the optical positions based on the CCD material. We find $\Delta\alpha$ = 4.2 $\pm$ 0.3 arcsec, and $\Delta\delta$ = 0.4 $\pm$ 0.3 arcsec, with an RMS error in the individual radio-optical differences of $\sim$ 0.8 arcsec. This RMS error suggests that the combined (1σ) uncertainty in the radio and optical positions will on average be between one and two arcseconds (as the shift was based on a subset of the "best" identification candidates). We adopt a 1σ uncertainty of 2 arcsec in the calculation of the likelihood ratio. The density of objects on the CCD images is estimated to be $\sim 2 \times 10^4$ deg^{-2}. With a search radius of four arcsec only one optical object unrelated to the radio source is expected to fall inside the combined search area of all the 14 RX objects with CCD finding charts; therefore the high accuracy of the radio and optical positions limits the contamination of the identification sample to an acceptable level.

The identifications were accepted if the likelihood ratio was > 4, a slightly lower cutoff than in the case of radio/X associations. Such a choice was possible because even with this lower $(LR)_{\rm min}$ the reliability is quite high. This, in turn, is due to the fact that the optical identification rate of RX objects turns out to be very high (see Table 3). The method described by De Ruiter et al. (1977) makes use of the a posteriori knowledge of $\theta_{\rm true}$ in the determination of R and C, and the higher $\theta_{\rm true}$ the more likely it is that there are no unrelated background objects among the proposed identifications. In fact, we find R = 0.99, so that not even one spurious object is expected among the proposed identifications listed in Table 3: although one background object is expected inside the combined search area, it will most likely lie at a larger distance from the radio position than a true radio/optical association. The completeness is C = 0.95: at most one identification may have been missed, because its LR happened to be below $(LR)_{\rm min}$. Since both R and C are close to one, the true and observed identification rates should be practically identical.

A summary of the search for optical counterparts of RX sources is given in Table 3. In columns 1 and 2 we give the X-ray and radio running number, in column 3 the optical morphological classification of the object closest to the radio position (g for galaxy, s for stellar), in columns 4, 5 and 6 the b and r magnitude and the $b-r$ color, in columns 7 and 8 the radio minus optical position differences in α and δ after application of the shifts in the optical position described above. An asterisk in column 9 means that the source was used for determining the shift in the optical positions. The likelihood ratio is given in column 10 and the acceptance of the identification, based on LR is indicated in column 11. In column 12 we give some extra information: the type of object based on spectroscopic information (Schneider, Schmidt and Gunn, private communication), and references to the comments at the bottom of the table.

Twelve of the sixteen RX sources of the 4σ sample have an optical counterpart, two have no optical identification on the CCD images and the remaining two have no identification on the POSS prints.

Table 4. POSS Optical identification of radio sources

R	Type	m_r	$\Delta\alpha$	$\Delta\delta$	Comments
1	?	20	–1.3	1.2	red object (r.o.)
6	G	18.5	1.9	2.4	r.o.
7	?	19.5	2.4	4.4	r.o.
8	G	19	–1.1	0.3	r.o.
9	G	18.5	–2.1	–0.3	see Table 3
25	S	18.5	0.1	1.1	b.s.o; see Table 3
27	G	16	–1.8	0.7	sp. gal., stellar nucl.
30	G	14.5	1.9	0.1	sp. gal.
31	G	19	0.3	1.5	r.o.
38	G	19	1.1	–0.6	r.o.
42	G	20	1.4	–0.4	r.o.
47	G	18.5	1.9	–2.5	r.o.
51	G	14.5	0.2	–1.3	ell. gal.
54	G	16	0.5	–1.4	ell. gal.
55	?	19.5	–1.7	–1.1	r.o.
57b	G	18	–3.4	–1.9	r.o.
68	G	17.5	1.3	0.1	ell. gal.
69	G	16	0.5	–1.4	sp. gal.
78	G	17	–0.7	–0.6	blue gal.
85	G	17.5	4.0	0.6	r.o.?
87	G	18.5	–1.1	0.3	r.o.
88	G	17.5	–3.1	0.4	r.o.
95	G	19.5	1.2	–2.7	r.o.

3.3. Optical identification of the entire 4σ radio sample

As a first step we used the Palomar Observatory Sky Survey (POSS) to search for optical counterparts of all the radio sources of the 4σ sample. Since this work will be followed in the near future by a more detailed study using the deeper CCD material, the optical identifications presented here should be considered as preliminary. Discussion of the quality of the identifications will therefore be postponed until the search for optical counterparts has been completed on the CCD images.

The identifications on the POSS of all the radio sources in the 4σ sample are summarized in Table 4. (For the purpose of optical identification we assumed that radio sources 57a,b and 111a,b each consist of two separate and unrelated sources.)

The meaning of the columns is clear. In this table we have listed all the objects visible on the POSS within a circle of $\sim$ 5 arcsec radius around each radio source. We have found 46

Table 4. (continued)

R	Type	m_r	$\Delta\alpha$	$\Delta\delta$	Comments
96	G	19	1.2	–0.6	r.o.
97	?	19	0.4	0.7	r.o.?
98	S	19	0.6	–2.3	b. o.
100	S	17.5	–0.6	–1.0	b.o.; see Table 3
102	G	16	–0.9	–1.2	ell. gal.
103	G	17	1.6	1.3	ell. gal., stellar nucl.
105	G	14.5	1.3	–2.6	gal., bright stellar nucl.
106	G	16.5	–1.1	0.0	compact gal.
111a	G	16	0.5	–0.6	sp. gal.
112	G	18	0.1	1.5	round ell. gal.
115	G	15.5	1.3	0.6	ell. gal.
117	?	19.5	0.8	0.6	r.o.
121	G	19.5	1.0	1.3	r.o.
122	S	15	–4.3	–1.1	b.o.
125	G	19	0.3	–0.1	r.o.
128	S	18.5	–0.3	–0.2	b.o.; see Table 3
129	G	16	0.5	1.1	ell. gal.
134	G	16	–0.7	1.3	b. compact gal.
135	?	19	–0.9	0.4	r.o.
136	?	20	0.5	0.6	r.o.
137	G	18	–0.1	–0.7	ell. gal.
140	G	16	–0.7	2.4	ell. gal.
149	S	18	–1.4	0.6	see Table 3

possible optical identifications, corresponding to $\sim$ 30 % of the 4σ sample. Preliminary analysis of the CCD data suggests that the final number of optical identifications will be at least twice as high.

4. Discussion

4.1. Counts and sky distribution of the radio sources

The 4σ sample contains 149 radio sources with flux density at 1.5 GHz $S > 120$ μJy (see Sect. 2.2), in an area of ~ 0.35 deg^2, corresponding to a surface density of almost 430 deg^{-2}, quite similar to the density of X-ray sources in the corresponding ROSAT image. Boyle et al. (1993, 1995) describe 20 cm radio observations of the Durham/AAT QSO survey field QSF3, which was also observed with ROSAT. While their X-ray limit is somewhat higher than ours ($\sim$ 4 against $\sim$ 2, in units 10^{-15} erg cm^{-2}s^{-1}), their radio image is a bit deeper than the Lockman Hole image. They detected 123 sources with a 20 cm flux density above 125 μJy within a radius of 18 arcmin, excluding two regions of 8 and 2 arcmin radius respectively (see Boyle et al. 1995). This corresponds to a surface density of $\sim$ 550 deg^{-2} at a $\sim 4.6\sigma$ level of 125 μJy, which is about 25 % higher than the Lockman Hole surface density. This difference is probably due to a larger incompleteness of the 4σ Lockman Hole sample (see the discussion in Sect. 2.2).

In order to reduce possible problems of incompleteness near the flux limit, we constructed the radio source counts considering only sources with a peak flux density at least five times the local RMS noise. The counts, normalized to a Euclidean distribution, are shown in Fig. 3, and are compared with a global fit to the source counts based on many different surveys (Windhorst et al. 1990). As is evident from Fig. 3, the Lockman hole data do not show any significant deviations, although they tend to lie below the global fit in the lowest flux bin. This slight offset in the counts near the flux limit is quite likely due to the fact that no resolution and completeness corrections were applied (see e. g. Oort & Windhorst 1985). Anyway, our counts are consistent with the apparent flattening of the normalized counts (corresponding to a *steepening* in the actual observed counts) that is present at sub-mJy levels in all 1.4 GHz counts presented by various groups (see e. g. Condon 1984; Windhorst et al. 1990; Boyle et al. 1993).

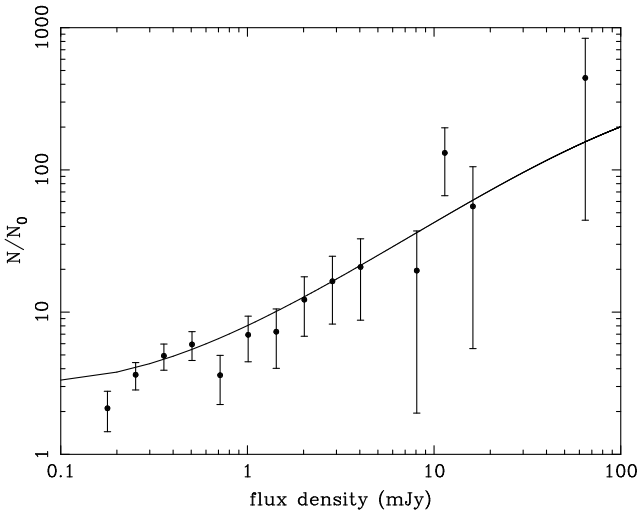

Fig. 3. The normalized radio source counts at 20 cm wavelength in the Lockman Hole region. Only sources with peak flux above 5σ were used. No resolution and completeness corrections were applied. For comparison a global fit to the counts, derived from many surveys (see Windhorst et al. 1990) is shown. The counts are normalized to $S^{-5/2}$ (Euclidean count).

The sub-mJy sources constitute the bulk of the Lockman Hole sample, and may represent, at least partly, a population of active or starburst galaxies (Thuan & Condon 1987; Windhorst et al. 1987; Benn et al. 1993). This opens the question whether we start to see also in the radio the underlying clustering of galaxies (see e. g. Oort 1987). In order to test the sky distribution we determined the two-point correlation function, using only sources with a flux density above 0.325 mJy: these can be seen in the whole 40 armin diameter region of the Lockman Hole image and thus we avoid problems due to the flux-dependent area of detectability of the fainter sources. The function $w(\theta)$ is shown in Fig. 4. Apparently some clustering at $\theta < 4$ arcmin is present, although each point is significant at a level of only $\sim 2\sigma$. However, the total number of observed pairs in the first four bins ($\theta < 4$ arcmin) is $\sim 5\sigma$ above the number expected on the basis of a random distribution ($N_{\rm obs}$ =191; $N_{\rm exp}$ =120), thus

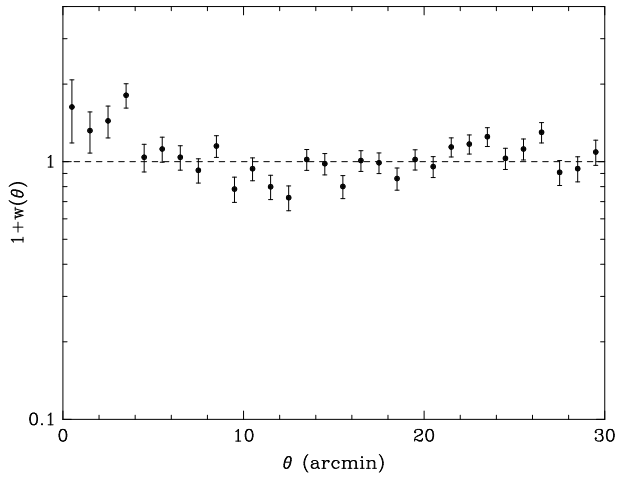

Fig. 4. The two-point correlation function $w(\theta)$, θ in arcminutes, for radio sources with $S_{1.5} > 0.325$ mJy (corresponding to the filled circles in Fig. 2).

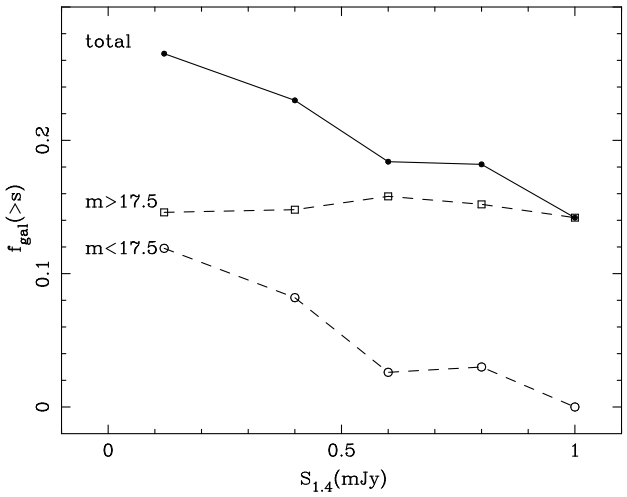

Fig. 5. Fraction of radio sources with flux density greater than S identified with galaxies, down to the limit of the Palomar Sky Survey, as a function of S. The full line shows all galaxies and the two broken lines indicate the fractions identified with faint ($m_r > 17.5$) and bright ($m_r \leq 17.5$) galaxies.

demonstrating the reality of the excess observed at these angular scales. Because of the low statistical significance of each data point we cannot make any definite statement about the slope of the correlation function, but it is interesting to note that the amplitude of the two-point correlation function agrees well with that found for optical galaxies with magnitudes in the range 18–19 (Neuschaefer et al. 1991), i. e. similar to the magnitudes of the bulk of our galaxy identifications. The filled circles in Fig. 2 clearly show the two rich "clusters" of radio sources which are responsible for the observed signal in $w(\theta)$ on the scale of a few arcmin.

4.2. Optical identification content of the radio source sample

As described in Sect. 3.3, we found optical candidates on the Palomar Observatory Sky Survey for $\sim$ 30 % of the 4σ radio sample. On the basis of the surface density of objects visible at the limit of the POSS we estimate that no more than 10 % of these identifications can be spurious. Our percentage of identifications is somewhat higher than the 19 % identification rate on UKST plates quoted by Boyle et al. (1993) for their sample. Also Windhorst et al. (1985) found a percentage of identifications lower than ours, down to roughly the POSS red magnitude limit.

A possible reason for this difference can be found if we divide the radio sources according to flux density, and use only galaxy identifications (quasars contribute at all flux levels about 10 % to the id-rate). At $S_{1.5} \leq 0.4$ mJy, 26 of 90 radio sources (29$\pm$6 %) have galaxy counterparts that are visible on the POSS prints (i.e. $m_r \leq 20$). Interestingly enough half of those (13 out of 26) are relatively bright galaxies with $m_r \leq 17.5$. Above 0.4 mJy the id-rate decreases to 23 ± 6 % (14 galaxy counterparts for 61 radio sources) and the difference becomes even more clear if we consider only sources with $S_{1.5} > 1.0$ mJy: only 4 of 28 radio sources (14 %) are now identified with galaxies on the POSS. In Fig. 5 we summarize these data, by plotting the cumulative fraction of radio sources identified with galaxies as a function of radio flux density: the rise in identification percentage at faint radio fluxes is clearly due to relatively bright galaxies.

A direct comparison can be made with the work of Windhorst et al. (1985) and of Oort (1987). Windhorst et al. (1985) have 23 radio sources (at 20 cm) below 0.4 mJy, of which 6 (26 %) are identified with galaxies; their id-rate is lower at higher fluxes, of the order of 16 %. Therefore the trend in the Windhorst et al. (1985) is similar to ours, and most of the difference in the overall id-rate is due to the fact that the large majority of the Windhorst et al. (1985) sources are stronger than 0.4 mJy, while in the present survey almost two thirds are below 0.4 mJy. Oort (1987) performed optical identifications of faint 20 cm radio sources in the deep Lynx.3A field. He noted a rise (like we do) from an overall id-rate of $\sim$ 20 % or slightly more at flux levels above 1 mJy to $\sim$ 32 % below $\sim$ 0.3 mJy. Since only 3 of the 24 identified radio sources at the lowest flux levels are associated with stellar objects his galaxy id-rate is close to 30 %. Oort (1987) used deeper CCD images with a limiting red magnitude of 21, but virtually all his identifications with the faintest radio sources would have been seen also on the POSS prints. However, most of them are fainter than m = 17.5. Unfortunately, in both studies the difference in id.-rate as a function of radio flux is not statistically significant due to the small number of objects involved.

We conclude that the data of Windhorst et al. (1987) as well as Oort (1987) are not inconsistent with the rise in identification percentage found by us below S = 0.4 mJy. However the increase described here is much more pronounced and appears to be mainly due to a population of relatively bright galaxies. Since the radio-optical associations are quite firm, there can be

no doubt as to the reality of this new population of nearby sub-mJy galaxies. Optical follow-up will have to decide whether we have picked up a nearby ($z \sim 0.1 - 0.2$) cluster, and reveal the nature of these galaxies.

4.3. The nature of the ROX sources

The 4σ radio sample produces 16 possible radio/X-ray associations, corresponding to an observed radio identification rate of ~ 12 %. On the basis of the completeness and reliability of this sample of possible associations, we estimate that the true identification rate is $\theta_{\rm true} \sim 10$ %, implying that about two of these radio/X-ray associations may be spurious. This is in agreement with the low identification rate of 8.7 ± 3.4 % reported by Boyle et al. (1995) and shows that there is little overlap between radio and X-ray sources at these low flux levels. A higher overlap between radio and X-ray sources has been found by Hamilton and Helfand (1993). In their cross–correlation between 2σ X-ray sources and VLA sources in two deep EINSTEIN fields, they found that about 18% of X-ray sources may be associated with radio sources. Although their radio flux limit is similar to ours, their X-ray limit, as judged by the surface density of their X-ray sources, is at least a factor five higher than ours. If we consider in our sample only the sources with an X-ray flux larger than 10^{-14} erg cm $^{-2}$ s^{-1} (38 sources), we find that eight of them (corresponding to 21%) are indeed associated with radio sources. Therefore, our data are in good agreement also with the Hamilton and Helfand result.

A similar trend of the percentage of radio/X-ray associations is present also with the radio flux. More than half of the RX sources have a radio flux density below 1 mJy, but this merely reflects the fact that the large majority of the radio sources in the 4σ sample are found at those levels. Actually, we find that of the 13 radio sources with $S_{1.5} > 2.6$ mJy seven (54 %) have an associated X-ray source, while only nine of the 136 fainter radio sources (7 %) have an X-ray counterpart.

In the three panels of fig. 6 we show the location of the 16 ROX sources in the planes of radio versus X-ray flux (Fig. 6a), X-ray flux versus magnitude (Fig. 6b) and α_{OX} versus α_{RO} (Fig. 6c). From inspection of these panels we see that:
a) There is no obvious correlation between radio and X-ray fluxes (panel a), although AGNs and galaxies appear to occupy different regions of the $S_{\rm R} - S_{\rm X}$ plane. All ROX galaxies have an X-ray flux below 1×10^{-14} erg cm $^{-2}$ s^{-1}, and most (4/5) even below 6×10^{-15} erg cm $^{-2}$ s^{-1}. Most of them (4/5) have also a relatively low radio flux, the only exception being the radio source R99 (associated to X116), which is a classical double radio source, with the highest radio flux in our sample. The optical identification is with a galaxy in a cluster. It is possible that the X-ray flux of this source is mainly due to the cluster rather than to the galaxy. As mentioned in Table 3, for this X-ray source there is an alternative optical identification with a very blue, probably stellar object, whose position is consistent with the position of one of the two radio lobes (R99b). Only future spectroscopic data and higher resolution radio data may help in resolving this uncertainty in the optical identification.

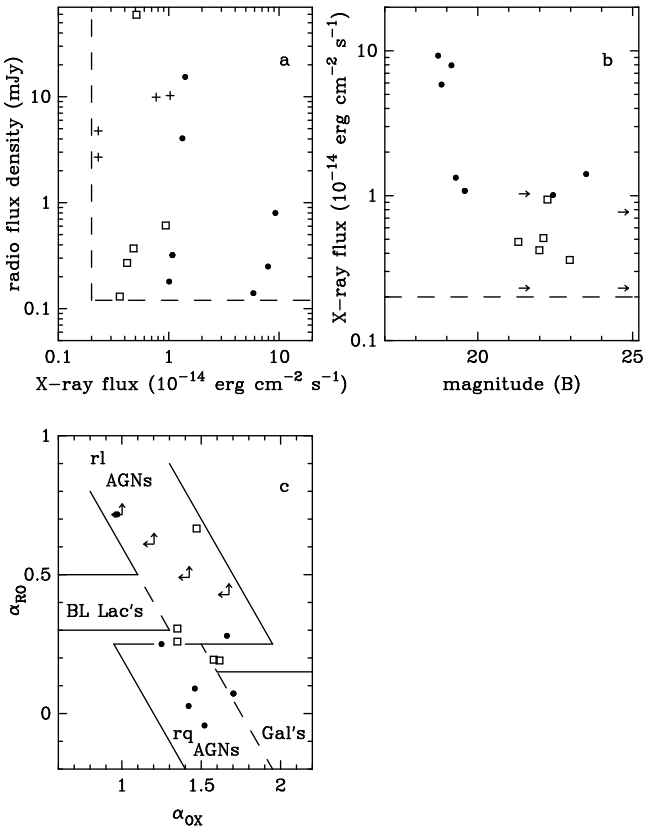

Fig. 6. a Radio flux density versus X-ray flux of RX sources (X-ray sources with a radio counterpart). Filled circles are AGNs, open squares galaxies, and crosses RX sources without optical identification. **b** X-ray flux versus blue magnitude (from CCD frames) of ROX sources. The arrows indicate the lower limits to the b magnitude on either POSS prints or CCD images for sources without optical id. **c** Radio-to-optical versus optical-to-X-ray spectral indices of ROX sources. The locations of various types of objects—BL Lac's, radio-loud and radio-quiet AGNs, and galaxies—, as determined from the EMSS, were taken from Della Ceca (1993).

b) The galaxies typically have a blue magnitude around 22, while the magnitudes of AGNs cover the entire range from 18 to 24 (panel b).
c) In the $\alpha_{\rm OX}$ versus $\alpha_{\rm RO}$ plane (panel c), the quasars nicely occupy the region where most of the AGNs of the Einstein Medium Sensitivity Survey (EMSS) lie (Della Ceca 1993), while the galaxies appear to be more "active" (i.e. with more radio and X-ray emission) than the typical galaxies detected in the EMSS. Note that also in this plane the radio source R99 (see point a) above) appears to be "anomalous". It is worth noting that the four RX objects, for which no optical counterpart is known, all fall in the region occupied by radio-loud AGNs. There is a good chance, therefore, that most, if not all, of them will turn out to be radio-loud AGNs.

We conclude that $\gtrsim 60$ % of the ROX sources are expected to be AGNs, while $\lesssim 40$ % are likely to be associated with "normal" galaxies (without active nuclei). Of course, future spectroscopic work may well reveal low level nuclear activity in some

of the objects which we are currently classifying as galaxies. A similar conclusion, i.e. more than 50% of RX sources are likely to be AGNs, was reached by Boyle et al. (1993) on the basis of their small sample of 5 RX sources in the QSF3 field. It is useful to stress that our result does not imply that the same percentages of AGNs and galaxies should be found in optical identifications of the overall faint X-ray population, irrespective of the radio flux. Unfortunately, no faint ROSAT sample with complete optical identifications exists yet. However, the existing samples with a high rate of identification (Shanks et al. 1991; Griffiths et al. 1995; Zamorani et al., in preparation) show that AGNs are $\sim 75\%$ and galaxies ≤ 15 % of the identified X-ray sources with $S_X \geq 5 \times 10^{-15}$ erg cm^{-2} s^{-1}, although the percentage of identifications with galaxies appears to increase at even fainter X-ray fluxes. Since the large majority of faint radio sources is associated with galaxies, the inclusion of the radio detection in the optical identification procedure obviously tends to increase the percentage of galaxies.

Among the AGNs, four have a blue magnitude < 19.5. They represent an AGN density of $\sim 12 \pm 6$ deg^{-2}, which is similar to the average density of optically selected AGNs at that magnitude. Beyond b = 19.5 the surface density of ROX AGNs (~ 25 deg^{-2} down to $b \sim 24$) quickly falls below that of optically selected AGNs (~ 110 deg^{-2} at $b \sim 22$, see Zitelli et al. 1992, and ~ 500 deg^{-2} at $b \sim 24$, estimated by Zamorani 1995). Assuming that, in agreement with the existing identifications in deep ROSAT fields, most of the X-ray sources in the Lockman field are AGNs, on the basis of Fig. 6c we can conclude that only a few percent of these X-ray selected AGNs are radio-loud. This is true even if all the objects without optical identification will turn out to be AGNs. At brighter X-ray fluxes, the percentage of radio-loud AGNs in X-ray selected samples is higher. For example, it is >10% in the EMSS sample. The decrease of this percentage at fainter X-ray fluxes was predicted by Della Ceca et al. (1994), on the basis of the luminosity functions and cosmological evolution of the radio-quiet and radio-loud AGNs in the EMSS.

In absence of spectroscopic data for the ROX sources identified with galaxies, we cannot say much about their nature. Some of them have blue colors, as expected from galaxies with strong starburst phenomena or with a Seyfert-like nucleus, but some have colors more typical of normal elliptical galaxies. It is likely that both types of galaxies are present in our sample, as already found by Griffiths et al. (1995) in their identification of faint ROSAT sources. Roche et al. (1995), cross-correlating the positions of faint galaxies with $< 4\sigma$ fluctuations in the unresolved X-ray background in five ROSAT fields, find some statistical evidence that a significant fraction of these fluctuations are associated with faint ($b \sim 23$) galaxies. Extrapolating to even fainter magnitudes, they conclude that galaxies may produce a contribution to the 1-keV background which is as large as that of QSOs. Although this conclusion still needs independent confirmation, the ROX galaxies discussed in this paper may be the "radio-loud" tail of these "X-ray loud" galaxies. In any case, since these ROX galaxies are also faint in the radio (with the exception of X116), they would be moderately low luminosity radio sources even at $z \approx 1$.

Acknowledgements. The National Radio Astronomy Observatory is operated by Associated Universities, Inc., under contract with the National Science Foundation. We thank R. Primavera, who carried out the astrometric measurements on the POSS prints. This work has received partial financial support from the Italian Space Agency (ASI contracts 92–RS–55 and 94–RS–96).

References

Benn, C.R., Rowan-Robinson, M., McMahon, R.G., Broadhurst, T.J., Lawrence, A. 1993, MNRAS, 263, 98
Boyle, B.J., Staveley-Smith, L., Shanks, T., G.C., Georgantopoulos, I., Stewart, G.C., Griffiths, R.E. 1995, Observatory, February 1995
Boyle, B.J., Staveley-Smith, L., Stewart, G.C., Georgantopoulos, I., Shanks, T., Griffiths, R.E. 1993, MNRAS, 260, 49
Condon, J.J. 1984, ApJ, 284, 44
Della Ceca, R. 1993, Ph.D. Thesis, University of Bologna
Della Ceca, R., Zamorani, G., Maccacaro, T., Wolter, A., Griffiths, R., Stocke, J.T., Setti, G. 1994, ApJ, 430, 533
De Ruiter, H.R., Willis, A.G., Arp, H.C. 1977, A&AS, 28, 211
Fomalont, E.B., Kellermann, K.I., Windhorst, R.A., Kristian, J.A. 1991, AJ, 102, 1258
Griffiths, R.E., Georgantopoulos, I., Boyle, B.J., Stewart, G.C., Shanks, T., Della Ceca, R. 1995, MNRAS, 275, 77
Hamilton, T.T., Helfand, D.J. 1993, ApJ, 418, 55
Hasinger, G., Burg, R., Giacconi, R., Hartner, G., Schmidt, M., Truemper, J., Zamorani, G. 1993, A&A, 275, 1
Kollgaard, R.I., Brinkmann, W., Chester, M. McMath, Feigelson, E.D., Hertz, P., Wielebinski, R., 1995, ApJS, 93, 145
Lockman, F.J., Jahoda, K., McCammon, D. 1986, ApJ, 302, 432
Mitchell, K.J., Condon, J.J. 1985, AJ, 90, 1957
Neuschaefer, L.W., Windhorst, R.A., Dressler, A. 1991, ApJ, 382, 32
Oort, M. J. A. 1987, Ph.D. Thesis, University of Leiden
Oort, M.J.A., Windhorst, R.A. 1985, A&A, 145, 405
Roche, N., Shanks, T., Georgantopoulos, I., Stewart, G.C., Boyle, B.J., Griffiths, R.E. 1995, MNRAS, 273, L15
Shanks, T., Georgantopoulos, I., Stewart, G.C., Pounds, K.A., Boyle, B.J., Griffiths, R.E. 1991, Nat, 353, 315
Thuan, T.X., Condon, J.J. 1987, ApJ, 322, L9
Warwick, R.S., Barber, C.R. 1992, proc. of the X-ray conference "X-ray emission from AGNs and the cosmic X-ray background", ed. W. Brinkman and J. Truemper, MPE report 235, p.242
Willis, A.G., De Ruiter, H.R. 1977, A&AS, 29, 103
Windhorst, R.A., Dressler, A., Koo, D.C. 1987, in IAU Symp.124 "Observational Cosmology", eds. A. Hewitt, G. Burbidge and L.Z. Fang, Dordrecht, Reidel, p.573
Windhorst, R.A., Mathis, D., Neuschaefer, L. 1990, in "Evolution of the Universe of galaxies", ASP Conference Series 10, ed. R.G. Kron, p.389
Windhorst, R.A., Miley, G.K., Owen, F.N., Kron, R.G., Koo, D.C. 1985, ApJ, 289, 494
Windhorst, R.A., Van Heerde, G.M., Katgert, P. 1984, AAS, 58, 1
Zamorani, G. 1995, in ESO workshop "Science with the VLT", ed. J.R. Walsh and I.J. Danziger, p.402
Zitelli, V., Mignoli, M., Zamorani, G., Marano, B., Boyle, B.J. 1992, MNRAS, 256, 349